



UNIVERSIDADE ESTADUAL DE CAMPINAS  
SISTEMA DE BIBLIOTECAS DA UNICAMP  
REPOSITÓRIO DA PRODUÇÃO CIENTÍFICA E INTELLECTUAL DA UNICAMP

**Versão do arquivo anexado / Version of attached file:**

Versão do Editor / Published Version

**Mais informações no site da editora / Further information on publisher's website:**

<https://link.springer.com/article/10.1007/s11666-019-00973-y>

**DOI: 10.1007/s11666-019-00973-y**

**Direitos autorais / Publisher's copyright statement:**

©2019 by Springer. All rights reserved.

DIRETORIA DE TRATAMENTO DA INFORMAÇÃO

Cidade Universitária Zeferino Vaz Barão Geraldo

CEP 13083-970 – Campinas SP

Fone: (19) 3521-6493

<http://www.repositorio.unicamp.br>



# Erosion–Corrosion Resistance of Laser Surface Alloying of NbC Thermal Spray Coatings on AISI 304L Steel

H. C. Fals<sup>1,2</sup> · A. S. Roca<sup>1</sup> · J. B. Fogagnolo<sup>3</sup> · L. Fanton<sup>3</sup> · M. J. X. Belém<sup>4</sup> · C. R. C. Lima<sup>4</sup>

Submitted: 28 June 2019 / in revised form: 18 October 2019 / Published online: 10 December 2019  
© ASM International 2019

**Abstract** NbC coatings were flame sprayed on AISI 304L substrates and further remelted using a 400-W power ytterbium-doped fiber laser (YLR-500-MM-AC-Y11), inserted into a chamber for argon atmosphere control. For the selection of the remelting parameters, isolated beads with remelting of the coatings were performed using three focal lengths and three remelting speeds. Using the selected laser parameters, layers were remelted with eight passes and 40% superposition. Erosion–corrosion tests were performed in a solution of NaCl in distilled water with SiO<sub>2</sub>. Surfaces and cross sections of the coatings were characterized by optical and scanning electron microscopy with dispersive energy microanalysis and x-ray diffraction. Microhardness measurements were taken in the cross section of the coatings. Modified surfaces 800 μm dense without pores or other defects and interfaces with the substrate of excellent metallurgical bonding were obtained. It was found that the dilution of the coating with the substrate formed a gradient of chemical composition and

mechanical properties. The erosive–corrosive wear resistance of the laser-remelted coatings was higher for the eroding impact angle of 90°. When the impact angle was 30°, the weight loss was higher and the ductile wear mechanism was conditioned by the formation of pitting on the modified surface.

**Keywords** erosion–corrosion · laser remelting · NbC coating · thermal spray

## Introduction

Compared with other methods of superficial modification, the process of obtaining superficial laser alloys (LSA) is distinguished by the possibility of obtaining superficial chemical compositions outside the equilibrium condition, also by the refinement and homogenization of microstructures, but better mechanical properties and generally greater resistance to wear and corrosion. This process solves still problems of the substrate–layer interface forming a metallurgical bond between the parts, and the thermally affected zone is small, minimizing the effects of the resulting stresses and deformations (Ref 1, 2). Laser surface alloys (LSAs) are usually obtained by surface fusing the substrate suitably coated by different methods. Carvalho et al. (Ref 3) pre-placed a 200 μm pure Nb on Ti-CP2 plate and melt with laser, obtaining a surface Ti alloy with lower stiffness and good quality. However, when the process is performed with powder previously placed on the substrate, a layer of the non-homogeneous alloying element is generally formed and difficult to control. In contrast, uniform surface layers of desired chemical compositions can be efficiently deposited by thermal spray.

This article is an invited paper selected from presentations at the 2019 International Thermal Spray Conference, held May on 26–29, 2019, in Yokohama, Japan, and has been expanded from the original presentation.

✉ C. R. C. Lima  
carlos.lima1@unimep.br; crelima@unimep.br

<sup>1</sup> University of Oriente, Av. Las Américas, s/n, 90400 Santiago de Cuba, Cuba

<sup>2</sup> Federal University of Technology- Parana, Ponta Grossa, PR, Brazil

<sup>3</sup> University of Campinas, Rua Mendeleyev, 200, Campinas, SP 13083-860, Brazil

<sup>4</sup> Methodist University of Piracicaba, Rod. Luis Ometto, Km 24, Santa Barbara d'Oeste, SP 13.451-900, Brazil

Thermal spray coatings generally present macrostructural heterogeneity with the formation of pores, voids, oxides, cracks and macrosegregation. To improve the performance of the coating layers, the laser remelting process has been widely used because it has the thermal characteristics and versatility necessary to control the geometry of the molten zone and the thermally affected zone.

Numerous investigations evaluate the application of the laser remelting on coatings obtained by thermal spray processes. Several laser-treated coatings can be found in the literature like tungsten carbides (WC-Co/NiCr) on AA 6082 T6 aluminum substrate (Ref 4), NiCrBSi autoclavable alloys on H13 steel (Ref 5, 6), ceramics (AL<sub>2</sub>O<sub>3</sub>-20%ZrO) on AISI 316L austenitic stainless steel (Ref 7), FeB on AISI 304L austenitic stainless steel (Ref 8), amorphous base coatings Fe (Ref 9), among others. Based on laser parameters, it has been proven that denser defect layers were obtained, with a thin microstructure, generally of superior hardness and wear resistance when compared to the original coating.

In recent decades, the use of surface modification with W (WC), Ti (TiC) and Ta (TaC) carbides has been remarkable in order to prevent wear and corrosion phenomena. However, the use of Nb carbide (NbC) has been poorly studied, although its physical and chemical properties indicate that it has excellent potential for applications where WC is currently the reference material (Ref 10–14).

Nb has already demonstrated the effect on the microstructure and properties of steels, cast iron (Ref 15) and Ti-CP2 (Ref 3). The beneficial effect of NbC precipitation during the thermomechanical processing of TWIP steels with high Mn and microalloyed to Nb was reported by Llanos et al. (Ref 16) and Li et al. (Ref 17), respectively. Zhi et al. (Ref 18) reported that Nb in the high hypereutectic iron Cr helped to decrease C in the liquid when formed the NbC, thereby transforming the primary carbides of M<sub>7</sub>C<sub>3</sub> type.

NbC (Ref 19) and NbC-Co (8%) with good fracture toughness and high non-lubricating wear resistance were obtained using spark plasma sintering (SPS). The fracture toughness increased when the Co concentration was 8-24% (Ref 20). Also, NbC-Ni SPS compounds had higher toughness when compared to NbC-Co compounds, but with lower hardness, which increased when NiMo and NiMo<sub>2</sub>C alloys were added (Ref 11). It has recently been shown that pure NbC and with Ni and Co as binding elements (NbC-Ni, NbC-Co) have excellent wear resistance under dry sliding conditions when compared to other ceramics and carbides (WC, Cr<sub>3</sub>C<sub>2</sub> and Mo) (C, N) (Ref 11, 19) and can even increase tool life (Ref 11) when compared to WC-Co. Tański et al. (Ref 21) applied Ta, Ti and Nb carbides by the laser remelting technique on tool steel surfaces of types

32CrMoV12-28 and X38CrMoV5-3, and dense and crack-free layers were obtained with high microhardness.

On the other hand, niobium is known to be one of the most biocompatible metals, but it has great potential for applications such as biomaterial. The evaluation of biocompatibility using cell viability tests indicated that there was no significant difference in NbC over a wide stoichiometric range compared to the alloy established with Ti-6Al-4V biomaterial (Ref 11). Both NbC and Nb<sub>2</sub>O<sub>5</sub> so far do not have REACH classifications related to human toxicology and are not listed as substances of great concern in opposition to Co<sub>3</sub>O<sub>4</sub> (Ref 11, 12). Based on the potentialities of NbC as a wear and corrosion-resistant material, together with the operational and thermal flexibilities of the laser surface alloy process, the aim of this work is to achieve a chemical gradient of Nb on the surface of AISI304L austenitic stainless steel that provides better mechanical properties and resistance to the wear and corrosion phenomena.

## Materials and Methods

### Thermal Spray Coating

In this study, the AISI 304L stainless steel plate (17.7 Cr, 7.9 Ni, 1.75 Mn, 0.32 Mo, 0.015 Si, 0.025 C, 0.006 S e 0.03 P) with 10 mm of thickness was used as substrate. High-purity NbC (CR-551 CBMM—*Companhia Brasileira de Metalurgia e Mineração*, Araxá, BR) powder was used to obtain the coatings. The NbC coatings were applied by low-pressure flame spray using a TeroDyn System 2000 (Eutectic Castolin, Wisconsin, USA), spray gun was used, and coatings with 250- $\mu$ m thicknesses were attained. The flame spray parameters are shown in Table 1. Just before spraying, the substrates surfaces were grit blasted with aluminum oxide to remove any impurity and impart a roughness to the substrate.

**Table 1** Flame spray parameters applied for NbC coatings

Powder feed rate	25 g/min
Standoff distance (SOD)	80 mm
Spray angle	90°
Oxygen pressure	38 Psi
Acetylene pressure	60 Psi
Air pressure	60 Psi
Spray velocity	140 mm/s

## Laser Remelting Process

A ytterbium-doped fiber laser (YLR-500-MM-AC-Y11) operating at a wavelength of 1.07  $\mu\text{m}$  with the approximation of the Gaussian beam distribution mode was used to produce chemical gradual surface in AISI304L. To find appropriate processing laser parameters with shapes characteristic near of the conduction mode, single laser beads with different parameters and energy densities were produced. The laser power was constant (400 W), and the laser speed as well as the defocusing distance of the laser beam was changed, as displayed in Table 2.

According to the experimental laser parameters, the diameter of the laser beam varied from 0.64 to 0.72  $\mu\text{m}$  and the energy density of the laser beam varied, in correspondence, from 12.8 to 28.8  $\text{J}/\text{mm}^2$ , as shown in Table 2. The selection of laser parameters to be used in continuous surface modifications was made using measurements of the geometry (width, height, depth) of the single beads. The measurements were taken using the image analysis technique. It was determined as an index (DW).

The remelting of the NbC coatings on the AISI304L substrate was carried out in an atmosphere control chamber (*MBraun, model MB 200 Modular*), with argon (99.95%) atmosphere to inhibit oxidation. A protective flux of 30 l/min argon was used in the remelting region during the process. Continuous coatings were obtained by overlapping the laser bead, using a distance between the laser bead centers equal to 400  $\mu\text{m}$ . A CNC  $x$ - $y$  table was used to control the laser speed and the overlapping ratio.

## Characterization of the Laser Remelting Surface

The microstructure and chemical composition obtained from the cross section of the flame-sprayed coating and laser-remelted zone were characterized by scanning electron microscopy (SEM) with energy-dispersive x-ray spectrometry (EDS). The backscattered electron mode was employed to enable chemical contrast in the SEM. The crystal structures of the NbC flame-sprayed coatings and

laser remelting surface were characterized by x-ray diffraction (XRD), and the analysis was carried out with a PANalytical X'Pert PRO diffractometer, using Cu-K $\alpha$  radiation source and scanned within  $2\theta = 20^\circ$ - $80^\circ$ . A Shimadzu microdurometer HMV 2T was used to perform microhardness measurements. The measurements were taken throughout the cross section of the samples.

## Erosive–Corrosive Wear Test

For the erosive–corrosive wear test, samples having dimensions 10  $\times$  23  $\times$  3 mm were prepared. The test was performed using a “mixing container” tribometer (Fig. 1). Quartz sand ( $\text{SiO}_2$ ) of particle size of 300/420  $\mu\text{m}$  was used as abrasive agent. Erosion–corrosion tests were performed in a solution of 3.5% NaCl in 1 L of distilled water with 300 g of  $\text{SiO}_2$ . During the tests, the samples were positioned at a  $30^\circ$  and  $90^\circ$  impact angle at 1550 rpm, equivalent to a particle impact velocity of 9.33 m/s. All the samples were polished with sand paper to 1200 mesh in order to reduce the characteristic surface irregularities. The total time of the tests was 3 h for each angle; after each running 0.5 h, the samples were removed from the device, washed, dried and weighed using a Shimadzu digital scale, model AY220, maximum weight of 220 g and precision of 0.001 g. The erosive–corrosive wear behavior of the coatings studied was evaluated in relation to the mass loss.

## Results and Discussion

### Microstructure and Phases Distribution

A chemical gradient of Nb resulted from the laser-remelted flame-sprayed NbC coatings on AISI 304L substrate. The NbC coatings presented a heterogeneous structure, with typical morphology in lamellar form, with partially molten particles, formation of oxides, pores and interlamellar voids, as can be observed in the details in Fig. 2.

**Table 2** Experimental laser parameters to obtain single bead

Laser power, W	Defocusing, mm	Laser speed, cm/min	Energy density, $\text{J}/\text{mm}^2$
400	0	10	25.6
		15	17.1
		20	12.8
	– 1	10	28.8
		15	19.2
		20	14.4
	1	10	28.8
		15	19.2
		20	14.4

**Fig. 1** (a) Tribometer; (b) toolholder and samples for 30° and 90° impact test angle; and (c) MEV image of the erosive particles

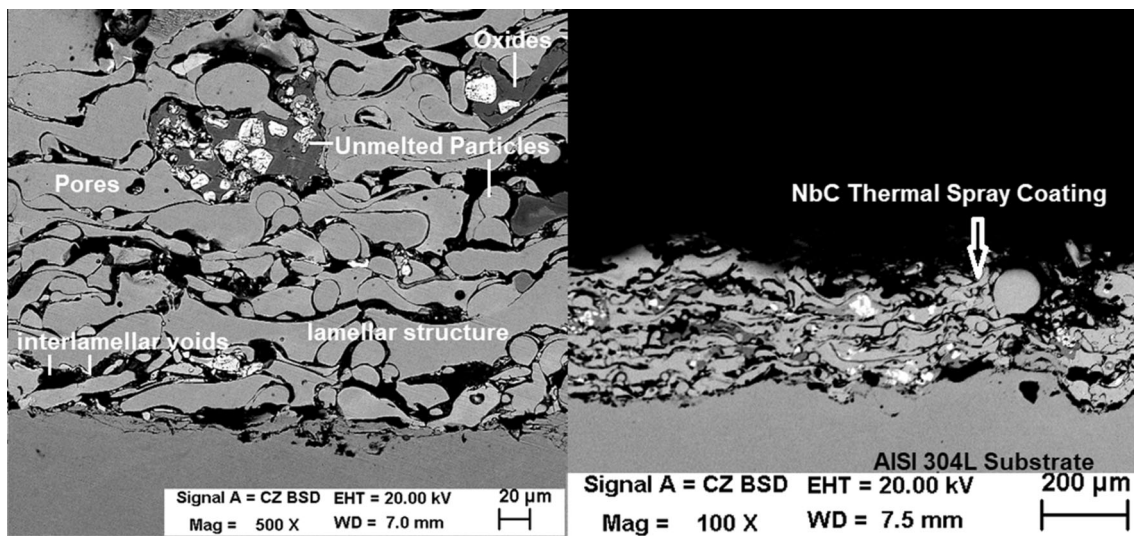
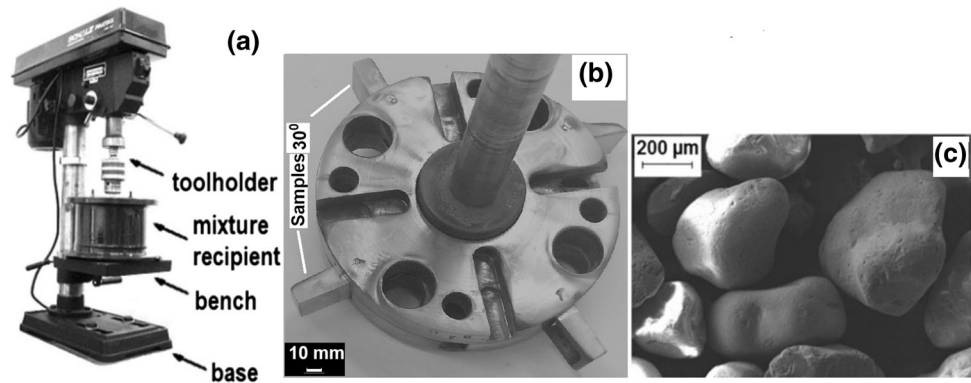


**Fig. 2** BSE-SEM cross-sectional images of the NbC thermally sprayed coating on AISI 304L substrate

Secluded beads with different laser parameters were initially performed on the samples of AISI 304L coated with NbC, varying the focal length (– 1, 0 and 1 mm) and the laser beam velocity (10, 15 and 20 mm/s) as shown in Fig. 3. Some porosity was found in the formation of the beads when 1 mm was used as the laser defocusing distance, that is, the focus inside the material. The formation of pores in this condition was probably caused by the generation of gas turbulence during the melting of the material in the root of the beads.

As expected, the laser parameters influenced the geometry of the beads mainly because of the variations in the heat input in the material determined by the energy density of the laser applied in each case, as can be observed in Fig. 3. The laser defocusing distance had a significant influence on the penetration of the beads; the lowest penetrations were obtained when the defocusing distance was – 1, regardless of the laser speed. Combining the results, the lowest penetration values were obtained when the laser speed was increased to 20 mm/s.

The study of the geometry of the beads is important in the processes of laser surface alloying, being well established that the processing of the material in the conduction mode is adequate to guarantee a stable geometry, free of defects and less influencing the substrate. The conduction mode is defined when the geometric relationship between the bead width and the depth of penetration (DW index) is less than 0.4 (Ref 3). The achievement of this mode depends on the parameters of the laser processing and occurs for conditions of low energy densities, also depending on the type of material to be processed.

Figure 4(a) and (b) shows graphs of response surfaces and iso-curves that correlate the behavior of the DW index with the laser speed and the defocusing distance. As shown in Fig. 4, DW indexes greater than 0.57 were obtained in the study. The lowest DW index value (0.57) was obtained in the condition of 20 cm/min and – 1 defocusing distance, the condition being closer to the driving mode. However, the energetic conditions planned in the work had the objective of achieving the dilution of the substrate to avoid the formation of cracks in the coatings due to the

**Fig. 3** Macrographic optic image of the beads with different laser parameters on AISI 304L coated with NbC

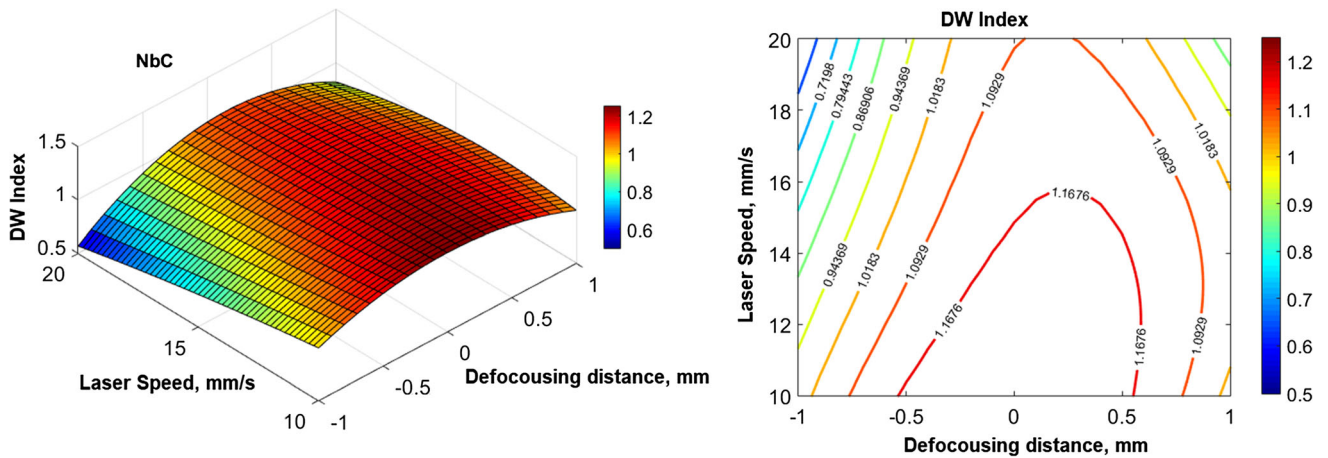
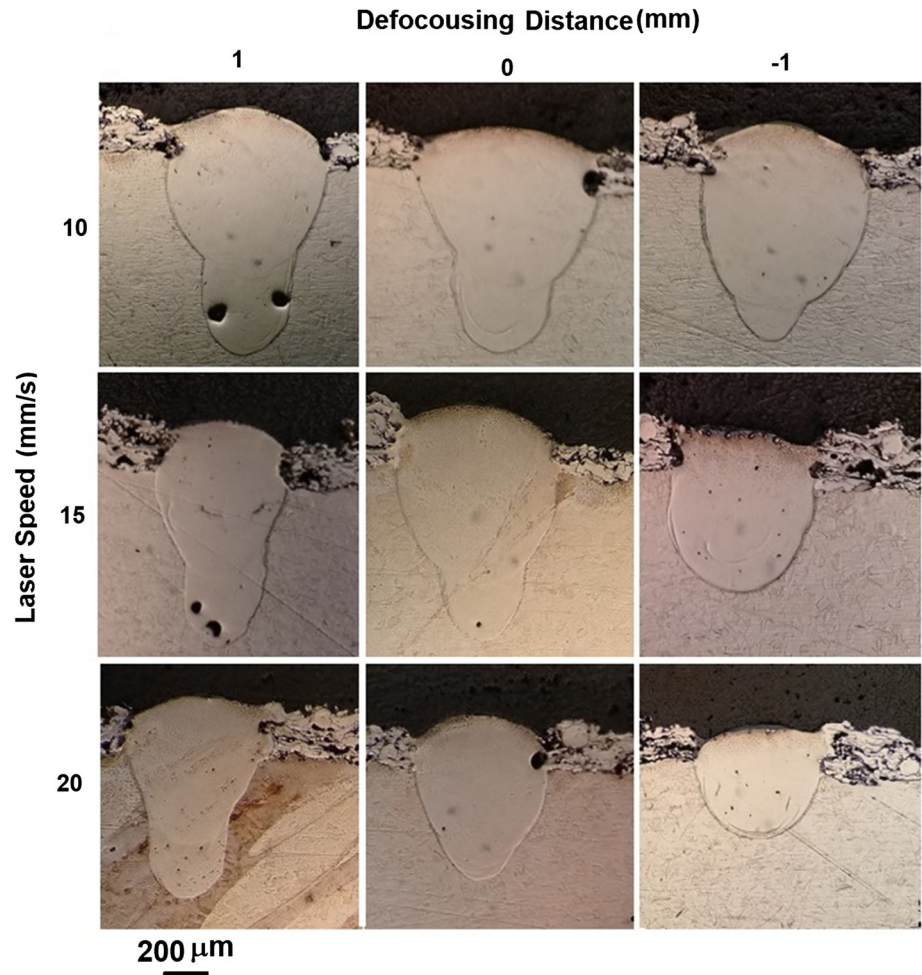


**Fig. 4** Correlation of the WD index with the laser parameters

stress–strain phenomena, besides forming a layer with gradual physic–chemical properties between the surface and the substrate.

In Fig. 4, it can also be seen that the highest values of the DW index were obtained for the focus on the surface

(defocusing distance 0), that is, with a smaller diameter of the laser exactly on the surface of the coating, and lower speeds of the laser, conditions with higher density of energy ( $62.5 \text{ J/mm}^2$ ). It was verified that, although the conditions with 1 and  $-1$  of defocusing distance have the

same energy density from the consideration of Gaussian behavior of the laser light ray, when  $-1$  was used as defocusing distance (focus 1 mm inside the material), the DW value was lower.

Figure 5(a) and (b) shows a scanning electron microscope image in the BSE mode of the NbC coating on the AISI 314L substrate, with laser velocity of 20 mm/s and in the condition of  $-1$  of defocusing distance, resulting in 406  $\mu\text{m}$  of penetration. The value of the DW index corresponds to the lowest one (0.57). In the backscattered electron image of Fig. 4(a), it is possible to verify a defect-free and chemical-contrast bead that allows identifying that there is no large compositional heterogeneity in the laser-processed coating. Since the atomic mass of Nb is higher than that of Cr, Ni and Fe, the regions with higher Nb content are revealed by their higher relative brightness, enlightening the Nb distribution throughout the remelted zone. Smaller darker regions of heterogeneity can be identified, which occur as a result of the high liquid metal convections formed during interaction with the laser beam.

Figure 5(b) shows the result of the chemical element mapping analysis (C, Cr, Fe, Ni and Nb) by ESD that was performed in the cross-sectional rectangle in the bead obtained by remelting with laser velocity of 20 mm/s in the condition of  $-1$  of defocusing distance and index DW 0.57. It was observed that, in these processing conditions, a good dilution of the coating material (NbC) and the substrate of AISI 304L were obtained, with homogenization of the Cr, Fe and Ni elements of the substrate and the concentration of Nb in the zone remelted by the laser.

After evaluating the morphology of the remelted beads using the DW index geometry analysis and testifying the dilution of the coating on the substrate and the homogenization of chemical elements in the beads, microhardness

profiles were obtained from the cross section of the beads obtained under defocusing distance of 1 and  $-1$  and speeds of 15 mm/s and 20 mm/s.

Figure 6 presents a graph of the microhardness variation in the cross section of the beads. It is observed that the microhardness of the remelted zone was higher than the substrate, regardless of the parameters of the laser processing used. The maximum microhardness values (355  $\text{Hv}_{0.1}$ ) were reached at 50  $\mu\text{m}$  from the surface of the samples processed with defocusing distance of  $-1$  and 20 mm/s.

In all the studied conditions, a microhardness gradient was verified between the surface of the remelted beads and the substrate, with microhardness values of about 210  $\text{Hv}_{0.1}$ . The increase in the microhardness in the remelted zone was influenced by the formation of fine solidification microstructures and out of equilibrium conditions, typical of high energy density and high solidification speed processes. Probably, as a consequence of the rejection of the Nb solute, CrNb intermetallic phases of greater hardness were formed in interdendritic regions. Continuous layers of laser surface alloying of NbC were obtained in AISI 304L, using the laser processing with laser speed of 20 mm/s,  $-1$  defocusing distance and 400 W of power, to obtain a DW index of 0.57, which constitutes the geometry relation closest to the conduction mode ( $\text{DW} < 0.4$ ). The obtained layers were produced using a 40% overlap.

Figure 7 shows a SEM image in the BSE mode of one of the layers obtained by laser remelting. The formation of a dense NbC + AISI 304L layer is confirmed with no defects and good metallurgical bonding with the substrate. In Fig. 7, the morphology of the remelted layer is observed; the consecutive deposits during the remelting are verified, and the thermal effect of the laser of the

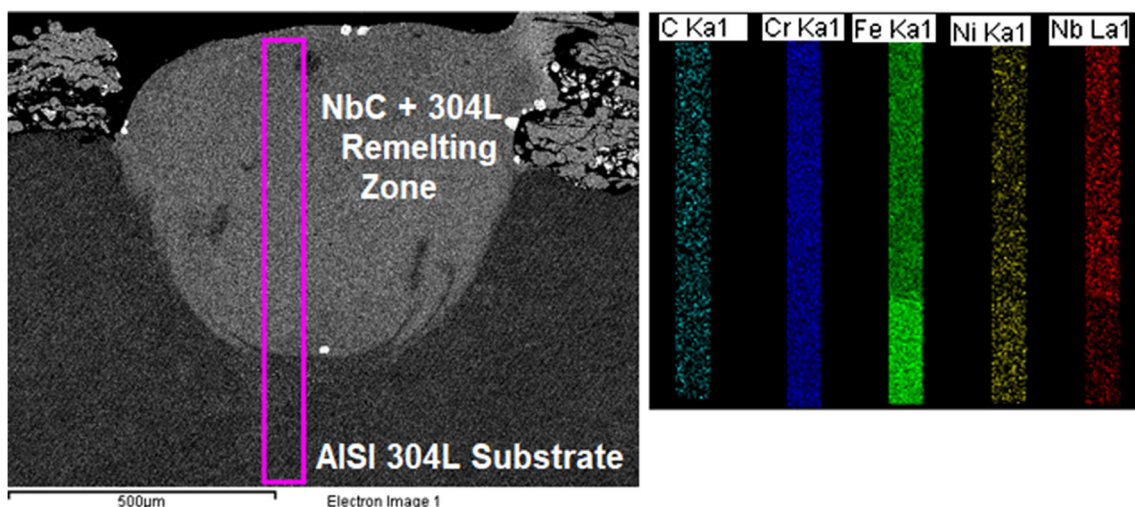


**Fig. 5** BSE-SEM images of single beads (a) laser speed 10 cm/min,  $-1$  defocusing distance, and (b) mapping of chemical elements by the EDS technique in the rectangle of Fig. 5a

subsequent deposits over the previous ones during the overlap of 40%. The subsequent passes remelted an area of the previous ones and also generated a thermally affected zone, with microstructural changes and consequent changes in the microhardness of the overlapping zone.

Figure 7(a) shows a detail of the solidification microstructure formed during the NbC remelting process on the AISI 304L substrate. In the SEM image (BSE mode), the fine dendritic microstructure formed in the zone is identified as a result of the solidification process. In the remelted zone, the formation of cellular and columnar

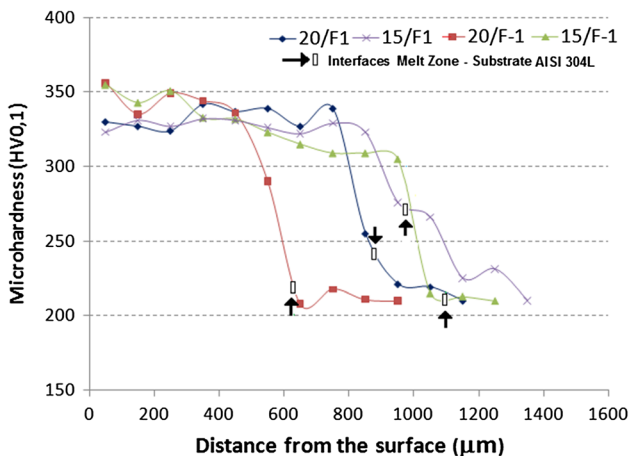


**Fig. 6** Microhardness profiles of single beads obtained from laser remelting of NbC coatings applied on AISI 304L substrates

dendritic structures resulting from the thermal gradients and the microstructure of the Nb, rejected at the solidification front, were observed.

The microstructure of the laser-remelted layer consists of a precipitation region (white) and the matrix (gray). The EDS analysis in the matrix and precipitation region (Fig. 7b) shows that the concentration of Nb in the matrix is between 0.46% and 0.62% by weight, and the concentration of Nb in the precipitation region is greater than 9% by weight, which is much higher than the average concentration of Nb in the matrix (Fig. 6b). Considering this concentration and the results of the XRD, it can be said that the white interdendritic phase is mainly the Laves intermetallic phase with formation  $(Ni, Fe, Cr)_2(Nb)$ .

The XRD diffractograms of the NbC-coated samples and the laser-remelted surface of the NbC-coated sample are shown in Fig. 8. The acquired diffractograms of the NbC thermal spray coating shown in Fig. 8(a) were compared to several others of NbC crystals from the Powder Diffraction File (PDF®) database, presenting very high compatibility with the NbC (PDF 38-1364 and 65-7993). There are also peaks related to the formation of Nb oxides (NbO, NbO<sub>2</sub> and Nb<sub>2</sub>O<sub>5</sub>) typical of the thermal spray process; these Nb oxides are compatible with PDF files 71-2146, 34-898 and 72-1484, respectively.

The XRD diffractograms of the laser-remelted surface are shown in Fig. 8(b) and have a good coincidence for the following four phases: (1) austenite phase of Cr-Ni steels (PDF 33-397)—(2) Laves phase (PDF 12-603), (3)

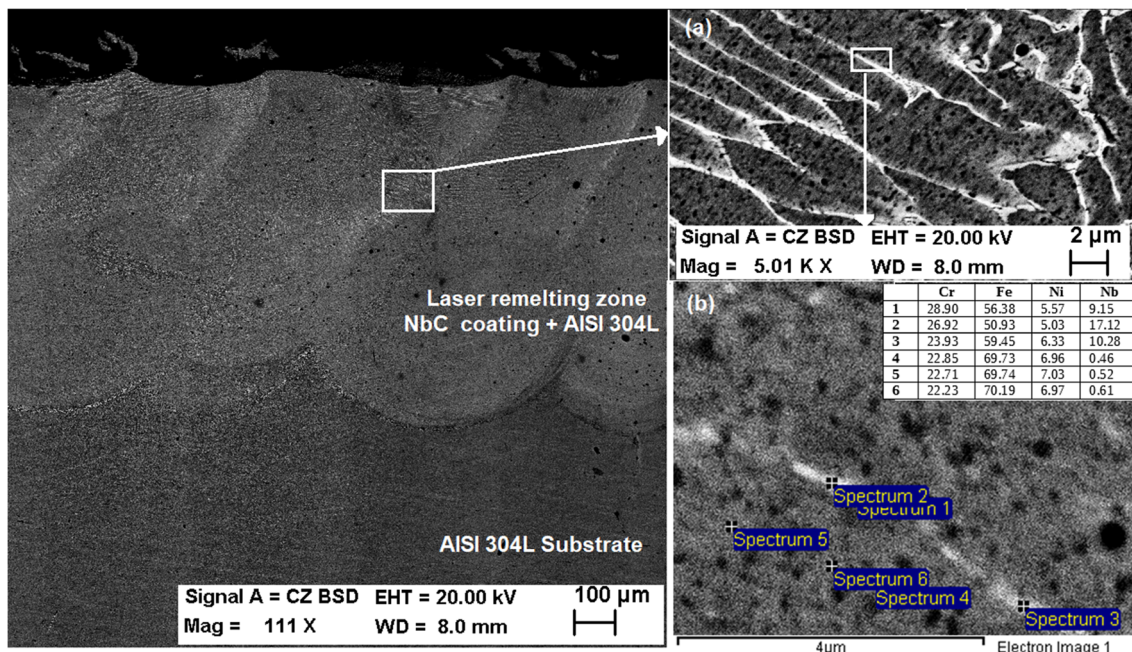


**Fig. 7** Laser-remelted continuous layer of the NbC + AISI 304L, (a) elongated dendritic arms in the laser-remelted zone and (b) punctual EDS analysis in different regions of the remelted zone

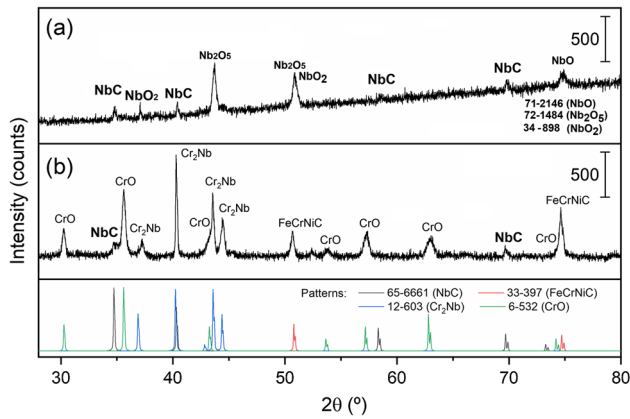


**Fig. 8** XRD diffractograms of the flame-sprayed NbC coating and the NbC + AISI 304L laser-remelted surface

chromium oxide (PDF 6-532) and (4) niobium carbide (PDF 65-6661).

The DRX corroborates the existence of the Laves intermetallic phase with formation of  $(\text{Ni, Fe, Cr})_2(\text{Nb})$ . There are also some NbC not dissolved during laser refusion, in addition to the austenite phase of AISI 304L steel and surface CrO, resulting from the heating process until fusion and generating the gradients of surface chemical composition.

### Erosion–Corrosion Results

Erosion–corrosion tests were carried out using a mixing vessel, in a solution of 3.5% NaCl and 300 g of  $\text{SiO}_2$  and adopting two impact angles of the erodent particles. The tests were performed to determine the weight loss of the NbC-remelted surfaces on AISI 304L substrate and AISI 304L steel without remelting. The results presented are only comparative, and further studies are needed to evaluate the synergy of the erosion–corrosion phenomena involved.

It is important to observe that the electrochemical measurements are the most used and indicated for the study of tribocorrosive phenomena (Ref 22). The mechanisms of corrosion-assisted wear are complex because the electrochemical state of the surfaces is highly dependent on the type and intensity of wear. Potentiodynamic polarization techniques make it possible to study the influence of wear on the active/passive performance of the surfaces and to estimate the kinetics that controls the corrosion rate.

Figure 9 shows the mean values of weight losses (mg) and wear rate of erosion–corrosion test. As can be observed in Fig. 9(a), the largest mass loss was 28.7 mg and occurred in the AISI 304L samples without surface modification and impact angle of  $90^\circ$ . When the impact angle was  $30^\circ$ , the mass loss decreased it in this same material reaching 21.7 mg. However, the NbC + AISI 316L laser-

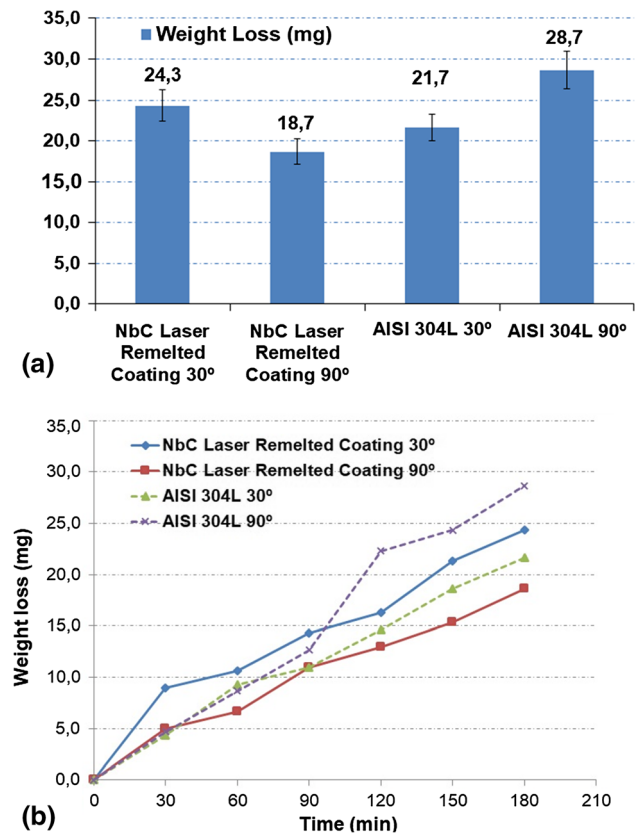


**Fig. 9** (a) Mass loss and erosion rate results from erosion–corrosion tests. (b) Wear rate of erosion–corrosion test

remelted samples with chemical and microhardness gradient formation showed the lowest mass losses (18.7 mg), when the impact angle of the erodent was  $90^\circ$ . In the remelted samples, when the impact angle was lower ( $30^\circ$ ), and mass losses increased up to 24.3 mg.

In the graph of the wear rate (Fig. 9b), it is possible to verify that in all conditions a gradual increase in wear occurred; however, it is observed that when the test time reached 90 min, a change occurred in the intensification of erosive–corrosive wear in the condition of  $90^\circ$  in the AISI 304L samples, probably caused by the cumulative effect of the degradation of the material by the normal impact of the erodent.

Figure 10 shows SEM images of the surface of the samples exposed to erosion–corrosion tests. In the samples with surfaces modified by the laser remelting process of NbC + AISI 304, pitting formation was observed after the erosion–corrosion test, as shown in Fig. 10(a). Pitting formation was observed on the surfaces independent of the erodent impact angle and was associated with the formation of the Laves phase on the modified surfaces, as previously proven. The formation of this intermetallic Laves phase  $(\text{Ni, Fe, Cr})_2(\text{Nb})$  causes a neighboring region with lower Cr concentration, as can be seen in the result of the

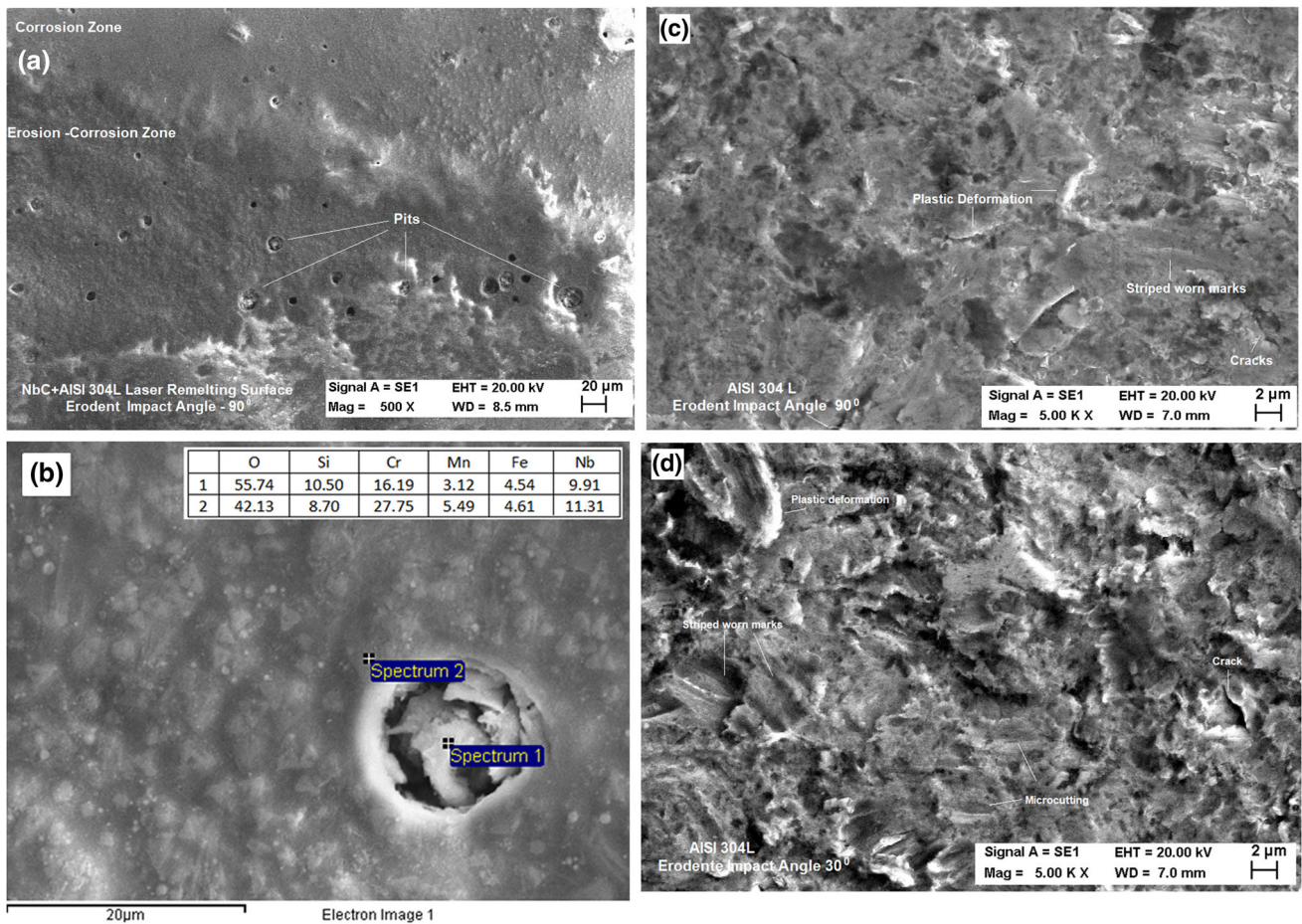


**Fig. 10** SEM images of erosive–corrosive wear surfaces, (a) formation of pitting at the surface of NbC laser-remelted samples on AISI 304L substrate and impact angle of 90°, (b) EDS analysis on pitting,

(c) erosive–corrosive wear surface of AISI 304L steel and impact angle of 90° (d) erosive–corrosive wear surface of AISI 304L steel and impact angle of 30°

EDS analysis shown in Fig. 10(b). As described by López et al. (Ref 22), the pitting formation does not directly cause significant increase in weight loss in the surface-modified samples; however, increasing the density of these cavities on the surface can aid the wear, reducing the resistance of some areas and resulting in greater weight loss. In the NbC + AISI 304L samples remelted with laser, an increase in the mass loss occurred when compared to the AISI 304L samples. This behavior was caused by the formation of superficial bites in this condition. When the angle of impact was 30°, the ductile mechanism of erosive failure prevailed with the formation of areas of high plastic deformation and micro-cuts; in this case, the formation of pitting increased the detachment of the material from the surface, that is, it had a synergistic effect in the total mass loss in the erosive–corrosive wear process.

In samples of AISI 304L steels with no surface modification, it was observed (Fig. 10c and d) a high surface roughness with the formation of multiple craters and overlapping deformed plates as the main erosion–corrosion

mechanism in AISI 304L steels (Ref 23). The surfaces of the materials suffer multiple impacts, leading to the formation of plastic-deformed areas in the form of lips, which can be removed by subsequent impacts of the erodent. In the erosion of AISI 304L steel, with impact angle of 30°, it was observed (Fig. 10d) greater plastic deformation caused by repeated oblique impacts.

It is also observed that the grooves produced by micro-cutting and plowing present the morphological characteristics of the erosion of ductile materials. When the impact angle of the erodent particles was 90°, as shown in Fig. 9(c), surface hardening has occurred, cracking to failure, and it can be speculated that corrosion increases erosion, accelerating the release of surface material by repeated impacts of particles.

The results obtained in these erosion–corrosion tests can be assumed as really promising for wear and corrosion applications of laser surfacing alloy of thermally sprayed coatings, mainly considering that most of the recent researches involving NbC coatings have been studied for

very thin films mainly applied by thermo-reactive deposition methods (Ref 24–26) with no perspective of use in large components.

Further specific corrosion evaluation for the laser-alloyed thermally sprayed NbC samples has been planned to better elucidate the corrosion mechanisms and the corrosion resistance in different industrial environments.

## Conclusions

The NbC coatings with a thickness of 250  $\mu\text{m}$  were flame sprayed on AISI 304L, and further laser remelted. The resulting surface layers were dense, free of defects and with excellent metallurgical bonding with the substrate. The layers showed a chemical gradient of Nb, Cr and Ni on AISI 304L substrate.

The laser surface modification of NbC coatings on AISI 304L substrate formed microhardness gradients between 350  $\text{HV}_{0.1}$  on the surface and 210  $\text{HV}_{0.1}$  on the substrate, depending on the energy density of the laser.

In the modified layers, the formation of thin dendritic microstructure of solidification showing dendritic arms with cellular or elongated morphology was observed, as a function of the thermal gradient and the segregation of Nb in the solidification front. Interdendritic regions rich in Nb generated the formation of the interleaved Laves phase ( $\text{NiFeCr}_2$  Nb).

The laser remelting of the AISI 304L steel with NbC generated layers with lower weight loss in erosion–corrosion tests applying the erodent impact angle of  $90^\circ$  when compared to the AISI 304 substrate. When the impact angle of the erodent was  $30^\circ$ , the weight loss was higher.

In the samples studied, a surface with evident effects of the erosion–corrosion process was observed, with formation of a region with a soft appearance and formation of pitting. The pitting formation was observed on the surfaces regardless of the angle of impact of the erodent and was associated with the formation of the Laves phase on the modified surfaces.

**Acknowledgments** Carlos Lima and Hipólito Fals acknowledge the support of São Paulo Research Foundation (FAPESP), Grant #2017/25363-0. Leonardo Fanton also thanks the support of FAPESP, Grant #2017/16715-0. This work was partially supported by the program FAP-UNIMEP, Grant #FAP-119/17. Special thanks are due to Professor Rubens Caran, from UNICAMP, for technical support.

## References

1. K.M. Mudali, R. Kaul et al., Influence of Laser Surface Alloying on Corrosion Resistance of Stainless Steel, *Mater. Sci. Technol.*, 2006, **22**(10), p 1185
2. R. Singh and N.B. Dahotre, Tribology of Laser Modified Surface of Stainless Steel in Physiological Solution, *J. Mater. Sci.*, 2005, **40**, p 5619-5626
3. L.R.A. Carvalho, E. Sallica-Leva, E.R. Encinas, and J.B. Fogagnolo, Less-Rigid Coating in Ti Obtained by Laser Surface Alloying with Nb, *Surf. Coat. Technol.*, 2018, **346**, p 19-28. <https://doi.org/10.1016/j.surfcoat.2018.04.038>
4. A. Gisario et al., Improvement of Thermally Sprayed WC–Co/NiCr Coatings by Surface Laser Processing, *Int. J. Refract. Met. Hard Mater.*, 2015, **52**, p 123-130
5. K.D. Dejun and B. Zhao, Effects of Loads on Frictionwear Properties of HVOF Sprayed NiCrBSi Alloy Coatings by Laser Remelting, *J. Alloys Compd.*, 2017, **705**, p 700-707
6. E.J. Chun et al., Laser-Assisted Selective Fusing of Thermal Sprayed Ni-Based Self-Fluxing Alloys by Using High-Power Diode Lasers, *Opt. Laser Technol.*, 2018, **100**, p 317-324
7. Y. Jianbing et al., Laser Remelting of Plasma-Sprayed Nanostructured  $\text{Al}_2\text{O}_3$ –20 wt%  $\text{ZrO}_2$  Coatings onto 316L Stainless Steel, *Appl. Surf. Sci.*, 2018, **431**, p 112-121
8. J. Chaoping et al., Improvements in Microstructure and Wear Resistance of Plasma Sprayed Fe-Based Amorphous Coating by Laser-Remelting, *J. Therm. Spray Technol.*, 2017, **26**(7), p 78-786
9. P. Shankar et al., Laser Modification of Detonation-Gun Sprayed Ferro-Boron Coatings on AISI, 304L SS, *Trans. Indian Inst. Met.*, 2010, **63**(4), p 751-756
10. M.G.D.V. Cuppari and S.F. Santos, *Phys. Prop. NbC Carbide Met.*, 2016, **6**(10), p 250. <https://doi.org/10.3390/met6100250>
11. M. Woydt et al., Potentials of Niobium Carbide (NbC) as Cutting Tools and for Wear Protection, *Int. J. Refract. Met. Hard Mater.*, 2018, **72**, p 380-387
12. M. Woydt et al., Niobium Carbide for Wear Protection: Tailoring Its Properties by Processing and Stoichiometry, *Met. Powder Rep.*, 2016, **71**(4), p 265-272
13. F.A.P. Fernandes, J. Gallego, C.A. Picon, G. Tremiliosi Filho, and L.C. Casteletti, Wear and Corrosion of Niobium Carbide Coated AISI, 52100 Bearing Steel, *Surf. Coat. Technol.*, 2015, **279**, p 112-117
14. N. Zhao, X. Yunhua, and F. Yonghong, Mechanical Properties of One-Step In Situ Synthesized NbC-Fe Composite Coating, *Surf. Coat. Technol.*, 2017, **309**, p 1105-1110
15. E.J. Chun et al., Microstructural Characterization of Ni-Based Self-Fluxing Alloy After Selective Surface-Engineering Using Diode Laser, *Appl. Surf. Sci.*, 2018, **442**, p 726-735
16. L. Llanos et al., Interaction Between Recovery, Recrystallization, NbC Strain-Induced Precipitation in High-Mn Steels, *Metall. Mater. Trans. A*, 2015, **46**, p 5248-5265
17. D. Li et al., Influences of Nb-Microalloying on Microstructure and Mechanical Properties of Fe–25Mn–3Si–3Al TWIP Steel, *Mater. Des.*, 2015, **84**, p 238-244
18. X. Zhi et al., Effect of Niobium on the As-Cast Microstructure of Hypereutectic High Chromium Cast Iron, *Mater. Lett.*, 2008, **62**, p 857-860
19. M. Woydt and H. Mohrbacher, The Use of Niobium Carbide (NbC) as Cutting Tools and for Wear Resistant Tribosystems, *Int. J. Refract. Met. Hard Mater.*, 2015, **49**, p 212-218
20. S.G. Huang, O. Biest, L. Li, and J. Vleugels, Properties of NbC–Co Cermets Obtained by Spark Plasma Sintering, *Mater. Lett.*, 2007, **61**, p 574-577
21. T. Tański et al., Thermal Fatigue Influence of Laser Treated Tool Steel Surface, *Proc. Eng.*, 2014, **74**, p 429-442
22. D.M. López et al., Use of Electrochemical Tests for Assessment of the Effect of Erosive Particle Size on the Erosion–Corrosion Behaviour of AISI, 304L Austenitic Stainless Steel, *Mater. Res.*, 2016, **19**(2), p 451-458

23. S.S. Rajahram et al., Erosion–Corrosion Resistance of Engineering Materials in Various Test Conditions, *Wear*, 2009, **267**, p 244-254
24. R. Soltani, M.H. Sohi, M. Ansari, A. Haghghi, H.M. Ghasemi, and F. Haftlang, Evaluation of Niobium Carbide Coatings Produced on AISI, L2 Steel Via Thermo-Reactive Diffusion Technique, *Vacuum*, 2017, **146**, p 44-51
25. W. Jin, Q. Meng, L. Niu, C. Li, and H. Wang, Properties of the Functionally Gradient Chromium-Niobium Carbide Coating Obtained by Thermo-Reactive Deposition Technique, *Key Eng. Mater.*, 2017, **753**, p 129-133
26. A. Amaya, O. Piamba, and J. Olaya, Improvement of Corrosion Resistance for Gray Cast Iron in Palm Biodiesel Application Using Thermoreactive Diffusion Niobium Carbide (NbC) Coating, *Coatings*, 2018, **8**(6), p 216

**Publisher's Note** Springer Nature remains neutral with regard to jurisdictional claims in published maps and institutional affiliations.